Journal Pre-proof

Novel distamycin analogues that block the cell cycle of African trypanosomes with high selectivity and potency

Jaime Franco, Laura Scarone, Marcelo A. Comini

PII: S0223-5234(20)30010-6

DOI: https://doi.org/10.1016/j.ejmech.2020.112043

Reference: EJMECH 112043

To appear in: *European Journal of Medicinal Chemistry*

Received Date: 11 November 2019

Revised Date: 3 December 2019

Accepted Date: 6 January 2020

Please cite this article as: J. Franco, L. Scarone, M.A. Comini, Novel distamycin analogues that block the cell cycle of African trypanosomes with high selectivity and potency, *European Journal of Medicinal Chemistry* (2020), doi: https://doi.org/10.1016/j.ejmech.2020.112043.

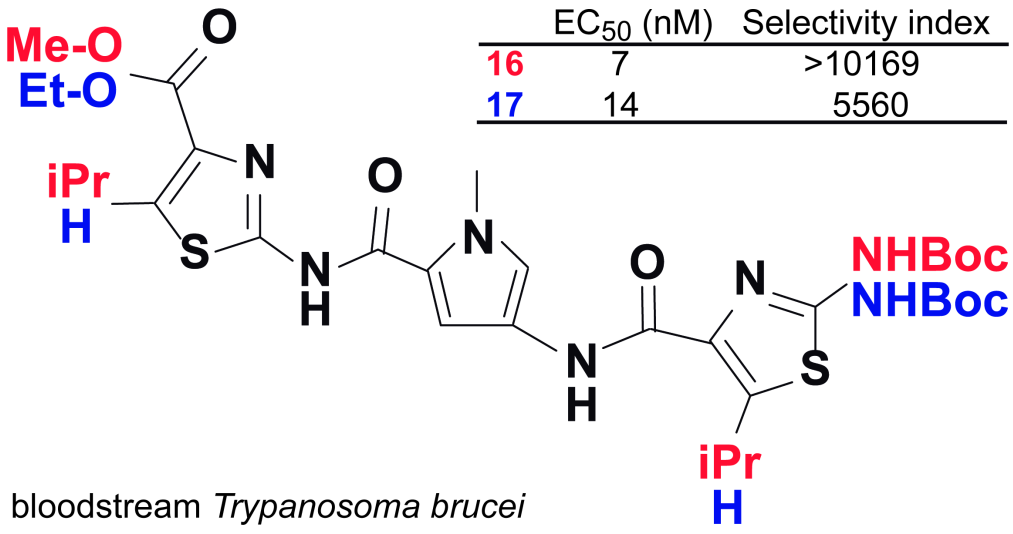

	EC_{50} (nM)	Selectivity index
16	7	>10169
17	14	5560

bloodstream *Trypanosoma brucei*

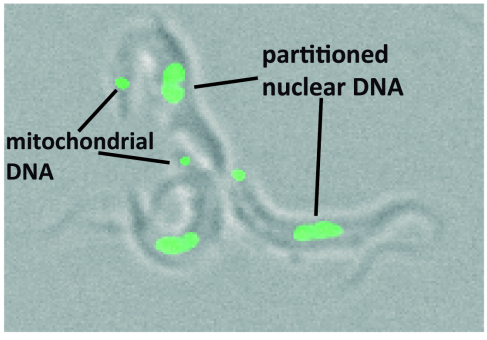

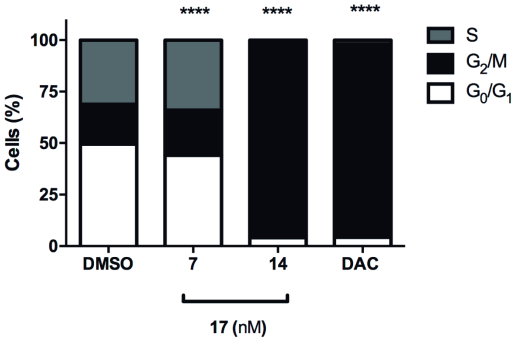

Novel distamycin analogues that block the cell cycle of African trypanosomes with high selectivity and potency

Jaime Franco[a,b], Laura Scarone[*a] and Marcelo A. Comini[*b]

[a] Laboratorio de Química Farmacéutica, Departamento de Química Orgánica, Facultad de Química, Universidad de la República, Montevideo, Uruguay.

[b] Group Redox Biology of Trypanosomes, Institut Pasteur de Montevideo, Montevideo, Uruguay.

* Corresponding authors:

(1) Laura Scarone

Laboratorio de Química Farmacéutica, Departamento de Química Orgánica

Facultad de Química, Universidad de la República

Gral. Flores 2124

Montevideo, CP 11800

Uruguay

E-mail: laurito@fq.edu.uy; Fax: +598 29241906; Phone: +598 29290290

(2) Marcelo Comini

Group Redox Biology of Trypanosomes

Institut Pasteur de Montevideo

Mataojo 2020

Montevideo, CP 11400

Uruguay

E-mail: mcomini@pasteur.edu.uy; Fax: +598 2522 4185; Phone: +598 2522 0910 ext. 164

Abstract

Polyamides-based compounds related to the Streptomycetal distamycin and netropsin are potent cytostatic molecules that bind to AT-rich regions of the minor groove of the DNA, hence interfering with DNA replication and transcription. Recently, derivatives belonging to this scaffold have been reported to halt the proliferation of deadly African trypanosomes by different and unrelated mechanisms. Here we describe the synthesis and preliminary characterization of the anti-trypanosomal mode of action of new potent and selective distamycin analogues. Two tri-heterocyclic derivatives containing a central *N*-methyl pyrrole ring (**16** and **17**) displayed high activity (EC_{50} <20 nM) and selectivity (selectivity index >5000 with respect to mammalian macrophages) against the infective form of *T. brucei*. Both compounds caused cell cycle arrest by blocking the replication of the mitochondrial DNA but without affecting its integrity. This mode of action clearly differs from that reported for classical minor groove binder (MGB) drugs, which induce the degradation of the mitochondrial DNA. In line with this, *in vitro* assays suggest that **16** and **17** have a comparatively lower affinity for different template DNAs than the MGB drug diminazene. Therapeutic efficacy studies and stability assays suggest that the pharmacological properties of the hits should be optimized. The compounds can be rated as excellent scaffolds for the design of highly potent and selective anti-*T. brucei* agents.

Keywords:

mitochondrial DNA; cytostatic; Trypanosoma brucei; minor groove binder; distamycin analogues; polyamides.

1. Introduction

African trypanosomiasis encompasses a group of zoonotic diseases caused by hemoflagellate parasites from different (sub)species of the Genus *Trypanosoma* that are endemic of the sub-Saharan region of Africa. The subspecies that causes Human African Trypanosomiasis (HAT), also known as African sleeping sickness, are *Trypanosoma brucei gambiense* and *Trypanosoma brucei rhodesiense*. Although control programs implemented by WHO have contributed to reduce the number of cases (< 10000 cases/year), 65 million people are at risk of contracting a disease that is fatal without therapeutic intervention [1,2].

T. b. brucei, *T. congolense* and *T. vivax* are responsible for Animal African Trypanosomiasis (AAT) [3]. Current estimations indicate that more than 3 million stock animals are affected by AAT, which accounts for large economic losses (several billions U$S/year) due to impaired productivity [4].

The current chemotherapy for HAT relies on old fashioned drugs (i.e. suramin, pentamidine, melarsoprol, eflornithine and nifurtimox) characterized by their limited, stage- and parasite subspecies-specific efficacy. Most of these drugs were developed based on empiric findings, are toxic and with undesirable administration routes [1,2]. In addition, the indiscriminate use of drugs to control AAT (e.g. isometamidium) has been linked to the emergence of cross-resistance with the human frontline drug pentamidine [5].

After 10 years of continued and joint efforts between academy, non-profit initiatives and pharma companies, the drug fexinidazole has been "rediscovered" and approved for the oral treatment of both the systemic and neurological stages of HAT [6]. Following a similar non-profit, R&D model, an acoziborole (SCYX-7158) has been selected as a promising pre-clinical candidate against HAT that is currently undergoing clinical studies [7]. To our knowledge, there are no more compounds in the clinical pipeline for this neglected disease.

Organic chemistry have been often inspired by the discovery of biological activities present in natural molecules. A good example is distamycin and netropsin, both being polyamides produced by the bacteria *Streptomyces netropsin* and harboring antifungal activity. Compounds of this family can bind into the minor groove of the DNA (hence named minor groove binder: MGB), especially in AT-rich regions, and by doing so interfere with DNA replication and transcription [8-11]. Several analogues have been synthesized and displayed potent anti-proliferative activity against a variety of biological models such as tumoral cells, viruses, fungi, bacteria and protozoan [12-18].

In the search for new MGB-like compounds acting against infectious organisms, Lang and *col.* reported a series of heterocycles linked by amide bonds some of which resulted active against *T. b. brucei*, in particular a molecule lacking a typical basic and flexible terminal group found in MGB [15]. Two years later, the same research group published on the anti-trypanosomal activity of a series of 32 structurally diverse MGB consisting of heterocycles linked by amide bonds [12]. Several of them presented a remarkable anti-proliferative activity (≤ 40 nM) and selectivity (>500) towards bloodstream *T. b. brucei*. A strongly fluorescent compound of this series displayed a granular distribution in the parasite cytosol with predominant signal accumulated in the nucleus and mitochondrial DNA (kinetoplast), as expected for compounds that interact with nucleic acids.

Recently, we have prepared and characterized a series of bi and tri-thiazoles resembling the distamycin scaffold **1** (**Figure 1**) [19]. The tri-thiazoles were more active and selective against infective *T. b. brucei* than the bi-thiazoles. Notably, the mode of action of the most potent (EC_{50} 310 nM) and selective (selectivity index = 16 *vs.* murine macrophages) hit, namely compound **1**, involved the loss of lysosome integrity but no effect on cell cycle.

Despite its potency, the low selectivity of **1** precluded advancing this compound to the next steps of the drug development pipeline. In order to obtain derivatives with a better biological profile and taking into account previous results with structurally related compounds, we hypothesized that inclusion of an *N*-methyl pyrrole as the central ring (**New series** shown in **Figure 1**) may confer a higher selectivity. To our surprise, this slight structural change yielded compounds far more potent (>26-fold) and selective (>340-fold), respectively, than **1**. Interestingly, the new hits inhibited parasite proliferation by blocking the replication of the kinetoplast. Despite the negative results obtained for one of the hits in therapeutic efficacy studies conducted on a mouse model of African trypanosomiasis, the new scaffolds appear as top candidates for optimization of their pharmacological properties.

2. Results and discussion

2.1. Chemistry and organic synthesis

In order to obtain a molecule with a *N*-methyl pyrrole as a central heterocyclic, we synthesized the trifluoroketone **2** [20,21] from the commercially available *N*-methyl pyrrole, which was nitrated in classical conditions to obtain the 2,4-disubstituted *N*-methyl pyrrole **3**.

Then, compound **3** was treated with NaH in aqueous medium to substitute the trifluoromethyl by an hydroxyl group [21] that led to the central building block **4** in very good yields.

We employed Hantzsch and Barton methodologies [22-24] to synthesize thiazoles **5** and **6**, that were derivatized to obtain two series of thiazoles containing esters and carboxylic acids with different protective groups on their 2-amino position **7-12**. (**Scheme 1**)

The *N*-methyl pyrrole **4** was coupled with the 2-aminothiazoles **5** and **6** in the presence of the iminium salt HBTU and DIPEA in CH_2Cl_2 at room temperature for 24 h obtaining **13** in 87 % yield and **14** in 62 % yield, respectively (**Scheme 2**). The nucleophilicity of the 2-amino thiazole has been reported as low due to the iminium tautomerism, in fact several reactions pointed that the endo nitrogen can be the nucleophile instead of the exo amino group [25,26]. This can explain the lower yield of **14** in comparison to **13**, whose isopropyl group likely increases the electron density and makes the 2-amino group more reactive towards the carboxylic group. As part of our studies, the HBTU activated acid of the *N*-methyl pyrrole was isolated, re-dissolved in dry THF and refluxed in the presence of compound **6** without increasing yields.

Next, the third heterocyclic ring (**9**, **10** or **12**) was coupled to **13** or **14** through the nitrogen at position 4 of the *N*-methyl pyrrole. Therefore a reduction of the nitro group was performed in the presence of H_2, Pd/C for 3 h resulting on a free amine on the position 4. Due to the reported instability of the pyrrole amine [27], the reaction crude was used without further purification. The crude was filtered through celite, concentrated *in vacuo* and re-dissolved in dry CH_2Cl_2 for coupling with carboxylic acids **9**, **10** and **12** in the presence of HBTU for 24 h (**Scheme 2**). Despite of being a two-step reaction, the tri heterocycles (**15** from **12** and **13, 16** from **13** and **9, 17** from **14** and **10**) were obtained in fair yields (e.g. 30 to 40 %). These three heterocycles were hydrolyzed in the presence of aqueous LiOH, leading to compounds **18-20** in excellent yields (**Scheme 2**).

2.2. Biological characterization

Compounds **13-20** were preliminary screened at a concentration of 5 µM against bloodstream *T. b. brucei* (**Table 1**). For compounds causing ≥ 75% parasite death at 5 µM, concentration-response assays against the pathogen and murine macrophages were performed to estimate EC_{50} and selectivity values.

As previously observed for the first series of compounds [19], two major features correlated positively with the biological activity of the second series: the number of heterocycles and the state of the terminal amine and carboxylic acid derivatives. Regarding the first factor, at 5 μM the bis-heterocycle (**13** and **14**) proved innocuous to trypanosomes while the tri-heterocyclic compounds (**15-17** and **19-20**), with the exception of **18**, exhibited a remarkable anti-parasitic activity (cell viability <25% at 5 μM). Protection of the carboxylic acid rendered the tri-heterocyclic compounds **15-17** (EC_{50} 827 to 7 nM) significantly more active than their corresponding un-protected analogues **18-20** ($EC_{50} \geq 3327$ nM). For both compound classes, the chemical nature of the group blocking the terminal amine (R_3) and the R_2 substituent affected the biological potency. For position R_3, the replacement of the acetyl group by a *t*-butyl carbamate increased in more than 60 times the potency of **16** (EC_{50} 12 nM) with respect to **15** (EC_{50} 827 nM), and at least twice for **19** (48 % viability at 5 μM) with respect to **18** (113 % viability at 5 μM). In contrast, the addition of an isopropyl group at 5 position of the thiazoles proved slightly detrimental for the anti-trypanosomal activity as evidenced by the lower activity of **16** (EC_{50} 12 nM) *vs.* **17** (EC_{50} 7 nM), and for **19** (48 % viability at 5 μM) *vs.* **20** (EC_{50} 3 μM). This suggests that addition of two isopropyl groups to the tri-heterocycles may interfere with the recognition of the molecular target. Interestingly, the replacement of the central azole ring of **1** (EC_{50} 310 nM) [19] by an *N*-methyl pyrrole increased significantly (26- to 44-fold) the anti-trypanosomal activity of the tri-heterocycles bearing a carbamated terminal amine and either propylated (**16**) or non-propylated (**17**) thiazoles.

Worth noting, **18** was previously synthesized and described as a potent growth inhibitor of bloodstream *T. b. brucei* (strain 427) with a minimum inhibitory concentration (defined as the concentration of compound that inhibited more than 20% parasite growth compared to non-treated control) of 64 nM [15]. However, under our experimental conditions (see section **4.6.1**), the compound lacked activity against the same strain and stage of *T. b. brucei*. In order to determine whether the different assay conditions were responsible for this conflicting data, **18** was assayed under conditions (initial density of 1.2×10^4 parasites/mL and 48 h treatment) resembling those reported in [15] (i.e. 2×10^4 parasites/mL and 48 h treatment) and including nifurtimox and **1** as positive controls. Under this less stringent assay condition and tested up to 60 μM, **18** resulted fully inactive whereas nifurtimox and **1** increased their EC_{50} by 20- and 5-fold (EC_{50} = 0.75 and 0.057 μM, respectively) when compared to the values obtained in our standard assay (5×10^5 parasites/mL and 24 h treatment, **Table 1**). Our finding is further supported by the fact that heterocycles with esterified azoles (**15-17**) are more

potent than the corresponding carboxylic acid analogues (**18-20**, **Table 1**). Thus, the data previously reported for **18** [15] remains intriguing.

Among the compounds displaying the most potent anti-trypanosomal activity (**15-19** and **20**), **16** presented an EC_{50} ~40 μM against murine macrophages, whereas the other ones lacked toxicity at a concentration of 120 μM [note that higher concentrations could not be tested due to low compound´ solubility at 1% (v/v) DMSO]. **16** and **17** displayed the highest selectivity indexes (SI): > 10169 and 5560, respectively. Similar to the effect observed against *T. brucei* and compared to the non-propylated analog **17** (EC_{50} for macrophages > 120 μM), propylation of the thiazoles of **16** (EC_{50} for macrophages ~39.5 μM) reduced by at least 3-fold macrophage toxicity. The replacement of the central thiazole ring by an *N*-methyl pyrrole impacted also positively in the toxicity against host cells, reducing it by 8-fold (i.e. EC_{50} against macrophages for **1** *vs.* **17** is 5 μM *vs.* ~40 μM, respectively).

In summary, the incorporation of a central *N*-methyl pyrrole to bis-thiazoles yielded derivatives significantly less cytotoxic and with higher anti-trypanosomal activity than the original tri-thiazoles analogs.

2.3. Mechanism of action

2.3.1. Cell membrane integrity

The remarkable improvement in the biological activity of several compounds from the new series with respect to **1** [19] raised the question whether this stem from an enhanced compound uptake, affinity for the molecular target and/or from a change in the mechanism of action (i.e. molecular target). To address this point, **16** and **17** were subjected to a thorough characterization of their trypanosomal killing mechanism.

Compound **1** has been shown to kill trypanosomes by disrupting the integrity of the lysosomal membrane, which is followed by release of toxic proteases, iron, generation of oxidative stress and permeabilization of plasma membrane [19]. Thus, we first investigated whether **16** and **17** would induce a similar phenotype in infective *T. brucei*. Both compounds added at their corresponding EC_{50} did not alter the integrity of the plasma membrane after a 4 h incubation, as observed by the lack of incorporation of the exclusion dye propidium iodide by the parasites (PI; **Figure 2A**). In contrast, a very low concentration of the detergent Triton X-100 (0.001 % v/v) damaged the membrane of 90% of the cells, an effect comparable to that exerted by **1** added at its EC_{50} and assayed under identical conditions [19]. Next, the capacity

of the compounds to induce oxidative stress at intracellular level was studied using a redox-reporter cell line of bloodstream *T. b. brucei*. The redox biosensor responds rapidly and specifically to changes in the ratio of reduced/oxidized glutathione and trypanothione (bis-glutathionylspermidine) [19,28,29], which are the major low molecular weight thiols in trypanosomes [30]. The level of oxidation of the redox biosensor was not significantly different for parasites treated with the vehicle or exposed to **16** or **17** at 1X or 5X their EC_{50} for 4 h (**Figure 2B**). This contrast with the behavior of **1**, which at concentrations $\leq EC_{50}$ induced intracellular oxidation [19], and strongly suggests that **16** and **17** possess a different mode of action.

2.3.2. Cell cycle analysis

As discussed above, several distamycin and netropsin analogs were described as MGB that, similarly to the natural products, bind to AT-rich regions of nucleic acids and thereby inhibit cell cycle progression [8]. On this basis and given the potent parasitostatic effect exerted by the new compounds, a potential interference with parasite cell cycle was studied. Before treatment with the compound, cell cycle synchronization was achieved by incubating the parasites with hydroxyurea for 6 h, which corresponds to the doubling time for non-treated infective *T. b. brucei*.

For this assay, we choose **17** as model compound of the new series and DAC, a well-known MGB, as control drug. After 24 h incubation, the distribution of parasites within the major phases of the cell cycle was estimated by measuring the DNA-content by flow cytometry (**Fig. 3**). For the DMSO-treated culture, cells were distributed in the following subpopulations: 49% in the growth phase (G_0/G_1), 31% in the synthesis phase (S) and 20% in the division/mitosis phase (G_2/M). Tested at its EC_{50} (7 nM), **17** produced a minor but statistically significant perturbation of the parasite´s cell cycle (i.e. G_0/G_1 phase: 44% cells, S-phase: 34% cells, and G_2/M-phase: 22%). Interestingly, doubling the concentration of **17** led to a more remarkable change with 94% of the trypanosomes arrested at the G_2/M phase and the remaining 6% at the G_0/G_1 phase. An almost identical effect was caused by DAC, which added at its EC_{50} (41 nM) blocked cell cycle at the division/mitosis (G_2/M-phase: 93% cells and G_0/G_1-phase: 7% cells).

2.3.3. DNA-content analysis by fluorescence microscopy

Kinetoplastid organisms are characterized for having a densely packed mitochondrial DNA (kinetoplast, K or kDNA) rich in AT-regions, and whose replication precedes that of the nucleus (N) and is perfectly synchronized with the cell cycle [31-33]. For instance, cells in the G1 or S phase of the cell cycle possess a single kinetoplast and a single nucleus (1K+1N). As the cell cycle progresses, the kinetoplast replicates and divides before the nucleus to produce a 2K+1N cell. Cells then enter mitosis, the outcome of which is a 2K+2N cell that, upon cytokinesis, divides into two 1K+1N siblings. To get a deeper insight into how **16** and **17** may interfere with this process, the nuclear and mitochondrial DNA organization was analyzed by epifluorescence microscopy (**Figure 4**). For DMSO-treated parasites, 80% of the cell population displayed 1K+1N (**Figure 4A, B**), which fully agrees with the results obtained for *T. brucei* grown under standard conditions [34] and confirms that the vehicle does not affect DNA replication. DAC treatment led to a major decrease in the 1K+1N cell population (44%, **Figure 4A**) and to the appearance of a large percentage of dyskinetoplastic trypanosomes (0K+1N: 39%, **Figure 4C**). Such phenotype has been reported for trypanosomes treated with different DNA-binding drugs, DAC among them, and ascribed to the linearization and protease-mediated degradation of the minicircle DNA, probably due to the inhibition of a mitochondrial type II topoisomerase [35-37]. For trypanosomes treated with **16** and **17**, the major population was also represented by 1K+1N cells (48% and 46%, respectively; **Figure 4A**). However, at variance with DAC, the second largest population (38% and 26% for **16** and **17**, respectively) corresponded to cells bearing a single kinetoplast and a single, but with a septum-like or partitioned, nucleus, a phenotype that we termed: 1K+1N* (**Figure 4A, D**). Thus, the distamycin analogues **16** and **17** appear to exert their trypanostatic effect by inhibiting the kDNA replication but without altering its structural integrity, as DAC and other MGBs do [35-37].

2.3.4. DNA-binding competition assays

The kDNA consists of concatenated maxi and minicircles encoding for rRNA and mitochondrial proteins, and for small guide RNAs, respectively [37, 38]. The minicircles are required for the editing of mRNA, are rich in A-T bases and, therefore, preferred targets of MGB [36-38]. As shown above, **16** and **17** interfere with the replication of the kDNA but do not lead to its degradation as MGBs do (**Fig. 4**). This suggests that, if any, the interaction of the distamycin analogues with the target DNA differs from that of the MGB. To test this, fluorescence competition assays were performed incubating a DNA-vector lacking (pUC18, 5

nM) or harboring a *T. brucei* minicircle sequence [38] (pUC18-kDNA, 5 nM) with an excess DAC, **16** or **17** (20 µM) for 30 or 120 min, followed by DNA-staining with DAPI (4',6-diamidino-2-phenylindole, 0.5 µM), a well-known fluorescent MGB with high affinity for A-T rich DNA [39]. DNA incubated with the vehicle DMSO and stained with DAPI was used as fluorescence normalization control.

The low fluorescence intensity of the DAC-treated samples (25-22 %) indicates that DAPI could not displace DAC-binding to either the plasmid and the minicircle DNA, even if incubation was extended from 30 min (**Fig. 5A**) to 120 min (**Fig. 5B**). This is in agreement with previous reports for MGB competitors [40,41] and confirms that DAC occupies DAPI sites in the DNA. At time point 30 min, **17** displayed certain preference for competing with DAPI-binding to the mock vector instead of the DNA containing the minicircle sequence (**Fig. 5A**). At this time point, **16** increased (15-28%) DAPI signal from both DNA samples when compared to the vehicle control. Interestingly, extending the incubation to 120 min, **16** and **17** diminished by 30% and 48%, respectively, the fluorescence of the DAPI-pUC18kDNA complex but not that of the mock DNA (**Fig. 5B**). This suggests that the interaction of **16** and **17** with the kDNA is a dynamic process.

Overall, the results supports that the interaction of **16** or **17** with the target DNA clearly differs from the MGB drug DAC. At shorter time points, **16** and **17** appear to have an overall relaxing effect on the DNA that favors dye incorporation to MG regions, whereas at longer incubation times both compounds are able to partially compete and/or allosterically affect dye-binding to DNA. Further experiments should be performed to confirm this preliminary finding.

2.3.5. Therapeutic efficacy test

Supported by the impressive performance of the compounds *in vitro*, a preliminary therapeutic efficacy study on a mouse model of African trypanosomiasis was conducted with **17**. Because the compound displayed a trypanostatic effect *in vitro*, the *in vivo* treatment was extended for one-week. Balb/cJ mice susceptible to *T. b. brucei* infection were infected with the parasite strain AnTaT 1.1, a pleomorphic cell line able to reproduce the natural infection [42]. Infected mice were divided in 4 groups (n = 6/group) that at day 4^{th} post-infection were treated with **17** given daily for 7 days at 1000X (8.36 mg/Kg) or 250X (2.09 mg/Kg) the EC_{50} determined *in vitro*, DMSO (3.3 mg/Kg × day/7 days) or a single dose of DAC (40 mg/Kg).

Parasitemia and animal status was monitored on a regular basis. For mice treated with vehicle (DMSO), parasitemia showed the typical behavior with a peak (mean value = ~100 million parasites/mL blood) at day 4th followed by a 2 to 3 orders of magnitude decrease between day 7-11 that can be associated to a temporary control of parasite proliferation by the host innate immune response [43]. From day 11th on, parasitemia raised steadily until the end of the assay (day 21st, **Fig. 6**). For mice treated with **17**, and independently of the dose administered, the parasitemia´ trend and absolute values were almost identical to those observed for the DMSO-treated group. This clearly indicates that **17**, even if given at 250-1000X its *in vitro* EC50, was unable to control *T. b. brucei* proliferation *in vivo*. In contrast, from day 7 onwards, a single dose of the control drug DAC was sufficient to reduce parasites from blood at levels undetectable by our counting method (detection limit $\geq 2.5\times10^4$ parasites/mL). Due to the lack of therapeutic efficacy of **17** and the high parasitemia levels, the experiment was finished at day 21st. For this time-window, and despite early (day 4th) deceases, each occurring in the DMSO and the 250X group, no differences in animal survival rate were observed among groups (Log-rank test, not shown).

The lack of correlation between *in vitro vs. in vivo* potency of **17** may be ascribed to different factors that likely have affected the bioavailability of the compound´s active form. Among them, metabolization by host´s hydrolases or oxidases may have converted **17** into a non- or significantly less-active species. In this respect, it is important to note that the tri-heterocyclics prepared in this work harbor two amide bonds, which may be susceptible to cleavage by liver esterases and amidases [44].

Among all these factors, we investigated *in vitro* a potential inactivation of **17** by serum components given that, although minor, a fraction of liver esterases is present in serum [45,46]. The compound (100 µM) was incubated for 24 h at 37 ºC with fresh or heat-inactivated (54°C for 45 min) fetal bovine serum and further added at different concentrations to *T. brucei* cultures. As shown in **Table 2**, in the absence of compound, either fresh or heat-inactivated serum did not impair parasite viability. At 10 nM, value close to compound´s EC_{50}, the anti-trypanosomal activity of **17** was fully abrogated or reduced by 30% when the compound was pre-incubated with heat-inactivated or fresh serum, respectively (p <0.01). Both serum samples were still capable to lower the activity of a 100-fold excess (1 µM) **17**. This result shows that serum component(s) may contribute to reduce the fraction of free or active compound.

3. Concluding remarks

A new series of distamycin analogues that are structure- and chemically-related to a scaffold from which several derivatives were identified as potent inhibitors of *T. brucei* proliferation [5-8] have been synthesized in good yields using classic organic chemistry reactions. Two tri-heterocyclic derivatives (**16** and **17**) displayed low nM potency against bloodstream African trypanosomes and high selectivity. In agreement with previous conclusions [9,19], our SAR analysis revealed that increased compound lipophilicity, due to the addition of a third heterocycle and blocking of the terminal amine and carboxylic acid with a carbamate and an ester group, respectively, are important determinants of compound activity. In fact, **16** (LogP = 3.7) and **17** (LogP = 2.4) have similar EC_{50} towards trypanosomes despite the first has two isopropyl groups and an increased LogP [47].

Our data highlights how minor changes in the structure of the distamycin scaffold may have a significant impact in the mode of action of related derivatives. For instance, the tri-thiazol **1** commits parasites to death by disrupting the integrity of the lysosome [19]. Here we show that replacement of the former central thiazol ring of **1** by an *N*-methyl pyrrole proved key in conferring the new analogues with a potent trypanostatic activity that involves the inhibition of DNA replication. In contrast to MGB drugs [35-37], **16** and **17** did not affect the structure of the kinetoplast but induced a partitioning of the nuclear DNA, which supports the blockade of DNA replication at a specific step. Interestingly, also *in vitro* **16** and **17** displayed low affinity for different template DNAs. Compared to the MGB-drug DAC, the compounds added in a 40-fold excess with respect to DAPI, only to a minor extent displaced dye-binding to a bacterial plasmid and *T. brucei* mitochondrial minicircle DNA.

Thus, the mode of action of **16** and **17** against trypanosomes clearly differ from that described for classical MGBs. The molecular targets of these compounds remain unknown. However, given the selectivity of **16** and **17**, the uniqueness of the trypanosomal mitochondrial DNA sequences and that kDNA replication is a major cell cycle checkpoint in these parasites, it is tempting to propose that components of the mitochondrial DNA replication machinery might be their potential molecular targets.

Despite **17** showed no activity in a mouse infection model of African trypanosomiasis, probably as consequence of its efficient and rapid inactivation by host's detoxication systems, the compounds characterized in this work represent excellent starting points for designing highly potent and selective anti-*T. brucei* agents.

4. **Experimental**

4.1. Chemical methods

IR spectra were recorded on a Shimadzu FTIR 8101A spectrophotometer. ^{1}H NMR and ^{13}C NMR spectra were recorded on a Bruker Avance DPX- 400 (see Supplementary Material). Chemical shifts are related to TMS as an internal standard. High resolution mass spectra (HRMS) were obtained on a MicroQ-TOF (ESI,Bruker Daltonics), low resolution mass spectra were obtained using a GCMS Shimadzu QP 1100-EX

Melting points were measured using a Fisher-Johns Melting Point Apparatus. Flash column chromatography was carried out with Silica gel 60 (J.T. Baker, 40 µm average particle diameter). All reactions and chromatographic separations were monitored by TLC, conducted on 0.25 mm Silica gel plastic sheets (Macherey/Nagel, Polygram SIL G/UV 254). TLC plates were analyzed under 254 nm UV light, iodine vapor, *p*-hydroxybenzaldehyde spray or ninhydrine spray. Yields are reported for chromatographically and spectroscopically (^{1}H and ^{13}C NMR) pure compounds.

All solvents were purified according to literature procedures [48]. All reactions were carried out in dry, freshly distilled solvents under anhydrous conditions unless otherwise stated.

4.2. General procedure for ester hydrolysis

An aqueous solution of LiOH or KOH [10% (w/v)] is added to a solution of the ester dissolved in THF or MeOH on a 1:1 ratio, the reaction is stirred at room temperature until TLC confirmed the disappearance of the ester. HCl [5% (v/v)] is added up to pH 2, the solution is extracted with EtOAc, dried over Na_2SO_4 and concentrated *in vacuo* to afford the corresponding acid.

4.3. General procedure for amide bond synthesis

HBTU (1.2 eq.), DIPEA (2 eq.) and 4-DMAP (0.2 eq.) are added under a N_2 atmosphere to a solution containing the amine (1.2 eq.) and the acid (1.0 eq.) on dry CH_2Cl_2 DCM at 0 °C. The mixture is stirred for 24-72 h at room temperature. AcOEt is added to the crude and the solution is washed with HCl [5% (v/v)] and then $NaHCO_3$ (sat), the organic layer is dried over Na_2SO_4, filtered and evaporated *in vacuo*. The crude is purified by flash chromatography using the corresponding eluent to give the amide.

4.4. General procedure for nitro reduction

The nitro compound is dissolved in EtOH and Pd/C (10 %) is added to the mixture, the reaction is carried at room temperature for 3 h under an H_2 atmosphere (3 atm). The crude is filtered through celite, concentrated *in vacuo*, redissolved in dry DCM and used without purification.

4.5. Building blocks

4.5.1. 2,2,2-trifluoro-1-(1-methyl-1H-pyrrol-2-yl)ethan-1-one (**2**)

N-methyl pyrrole (5.4 g, 67 mmol) is dissolved in 18 mL of dry Et_2O under a N_2 atmosphere, the reaction is then cooled to 0 ºC on an ice bath. TFAA (9.4 mL, 67 mmol) is added slowly and the reaction is stirred for 6 h at 0 ºC. The reaction is washed with $NaHCO_3$ [10% (w/v); 3 x 40 mL] and brine (2 x 10 mL). The organic layer is dried over Na_2SO_4, filtered and concentrated *in vacuo*. Yellow oil. Y = 98 %. ^{1}H-NMR ($CDCl_3$, 400 MHz): δ 3.98 (s, 3H), 6.26 (dd, *J* = 4.6 , 2.3 Hz, 1H), 7.04 (m, 1H), 7.22 (dd, *J* = 4.6, 2.3 Hz, 1H).

4.5.2. 2,2,2-trifluoro-1-(1-methyl-4-nitro-1H-pyrrol-2-yl)ethan-1-one (**3**)

Once compound **2** (11 g, 67 mmol) is dissolved on acetic anhydride, HNO_3 is added dropwise (5.6 mL, 0.134 mmol) keeping the reaction at - 5 ºC. After addition, the reaction is stirred for 3 h at 10 ºC. $CHCl_3$ is added and the mixture is extracted exhaustively with $NaHCO_3$ [10% (w/v)], then the organic layer is dried over Na_2SO_4, filtered and concentrated *in vacuo*. Orange oil. R = 80 %. ^{1}H -NMR ($CDCl_3$, 400 MHz): δ 4.06 (s, 3H), 7.69 (s, 1H), 7.82 (s, 1H).

4.5.3. 1-methyl-4-nitro-1H-pyrrole-2-carboxylic acid (**4**)

Compound **3** (1 g, 4.5 mmol) dissolved in 20 mL of DMF:H_2O (9:1) and added dropwise to a solution containing NaH (0.43 g, 18 mmol) in 5 mL of dry DMF and then heated at 60 ºC for 3 h. HCl [5% (v/v)] is then added to the solution and the pH is adjusted at a value of 2, the aqueous layer is extracted with Et_2O. White solid. R = 86 %. M.p.: 204-205 °C [49]. ^{1}H-NMR ($CDCl_3$, 400 MHz): δ 4.19 (s, 3H), 7.26 (d, *J* =2.0 Hz, 1H,), 8.23 (d, *J* =2.0 Hz, 1H), 13.16 (s, 1H). ^{13}C-NMR ($CDCl_3$, 100 MHz): δ 37.9, 111.8, 124.3, 129.6, 134.5, 161.5.

4.5.4. Ethyl 2-aminothiazole-4-carboxylate (**5**)

Compound **5** is prepared according to the literature [15]. White solid. Y = 80 %. M.p.: 171-174 °C [50]. ^{1}H-NMR (400 MHz, $(CD_6)_2CO$): δ 1.31 (t, *J* = 7.2 Hz, 3H), 4.25 (q, *J* = 7.2 Hz, 2H), 6.82 (s, 2H); 7.44 (s, 1H). ^{13}C-NMR (100 MHZ, $(CD_6)_2CO$): 14.6, 60.9, 117.5, 144.1, 161.9, 169.2.

4.5.5. Methyl 2-amino-5-isopropylthiazole-4-carboxylate (**6**)

Compound **6** is prepared according to the literature [18,19]. Yellow oil. Y = 50 %. ^{1}H-NMR (400 MHz, $CDCl_3$): δ 1.27 (d, *J* = 7.0 Hz, 6H); 3.88 (s, 3H); 4.07 (m, *1*H), 5.18 (s, 2H). ^{13}C-NMR (100 MHz, $CDCl_3$): δ 24.8, 27.6, 51.9, 134.6, 150.6, 162.7, 163.2.

4.5.6. Methyl 2-((tert-butoxycarbonyl)amino)-5-isopropylthiazole-4-carboxylate (**7**)

Compound **6** 2.5 g (12.5 mmol) is dissolved in 40 mL of dry CH_2Cl_2 under a N_2 atmosphere. TEA (5.3,37 mmol), Boc_2O (8.175 g, 37 mmol) and 4-DMAP (cat) are added to the mixture. The reaction is refluxed for 6 h, and then 200 mL of EtOAc are added, the reaction is washed with HCl [5% (v/v); 3 x 15 mL] and H_2O (50 mL). The organic layer is dried over, filtered and concentrated *in vacuo*. The crude is purified by flash chromatography using EtOAc:Hexanes (1:4) as eluent. White solid. R_f = 0.4. Y = quantitative. M.p.: 140-141 °C. ^{1}H-NMR ($CDCl_3$, 400 MHz): δ 1.34 (d, *J* = 7.9 Hz, 6H), 1.50 (s, 9H), 3.90 (s, 3H), 4.16 (m, 1H). ^{13}C NMR ($CDCl_3$, 100 MHz): δ 24.9, 27.7, 28.0, 52.0, 84.7, 135.6, 149.7, 154.3, 159.1, 162.6.

4.5.7. Ethyl 2-((tert-butoxycarbonyl)amino)thiazole-4-carboxylate (**8**)

Compound **5** (0.439 g, 2.5 mmol) is dissolved in 10 mL in DCM:THF (1:1) under a N_2 atmosphere. $(Boc)_2O$ (0.577 g, 2.65 mmol), TEA (0.744 g, 7.36 mmol) and 4-DMAP (cat) were added and the reaction was refluxed for 72 h, then the solvent was removed *in vacuo* and redissolved in EtOAc, washed with HCl [5% (v/v); 3 x 15 mL], dried over Na_2SO_4, filtered and concentrated *in vacuo*. The residue was purified using flash chromatography using EtOAc:Hexanes (3:7) as eluent. White solid. R_f = 0.38. R = 74 %. M.p.: 105-106 °C. ^{1}H-NMR (400 MHz, (Acetone-d_6): δ 1.33 (t, J = 7.2 Hz, 3H), 1.54 (s, 9H), 4.30 (q, *J* = 7.2 Hz, 2H), 7.92 (s, 1H), 10.37 (s, 1H). ^{13}C-NMR (100 MHz, (Acetone-d_6): δ 14.6, 28.2, 61.1, 82.2, 122.4, 142.8, 153.1, 160.4, 161.

4.5.8. 2-((tert-butoxycarbonyl)amino)-5-isopropylthiazole-4-carboxylic acid (**9**)

Compound **9** was obtained from **7** using the ester hydrolysis general procedure. White solid. Y = 100 %. M.p.: 132-133 °C. ^{1}H-NMR (DMSO-d_6, 400 MHz) δ 1.25 (d, *J* = 7.2 Hz, 6H), 1.46 (s, 9H), 3.99 (m, 1H), 11.54 (s, 1H), 12.62 (bp, 1H). ^{13}C-NMR (DMSO-d_6, 100 MHz) 25.1, 27.2, 28.3, 81.8, 135.5, 150.0, 153.6, 155.4, 163.9.

4.5.9. 2-((tert-butoxycarbonyl)amino)thiazole-4-carboxylic acid (**10**)

Compound **10** was obtained from **8** using the ester hydrolysis general procedure. White solid. Y= 100 %. M.p.: 112-113 °C. ^{1}H-NMR (400 MHz, DMSO-d_6): δ 1.48 (s, 9H), 7.92 (s, 1H), 11.71 (s, 1H), 12.73 (s, 1H).^{13}C-NMR (100 MHz, DMSO-d_6): δ 27.9, 81.6, 121.9, 142.4, 153.1, 159.6, 162.4.

4.5.10. Methyl 2-acetamido-5-isopropylthiazole-4-carboxylate (**11**)

Compound **9** (118 mg, 0.588 mmol) is dissolved under a N_2 atmosphere in dry CH_2Cl_2 (4 mL) on an ice bath. Pyridine and Ac_2O in excess and 4-DMAP (cat) are added to the mixture. The reaction is then refluxed for 6 h and then EtOAc is added, the reaction is washed with HCl [5% (v/v); 2 x 10 mL], and H_2O (15 mL). The organic layer is dried over Na_2SO_4, filtered and concentrated *in vacuo*. The crude is purified in silica flash chromatography using EtOAc:Hexanes (4:1) as eluent. White solid. R_f = 0.48. Y = 83 %. M.p.: 97 ºC. ^{1}H-NMR ($CDCl_3$, 400 MHz): δ 1.34 (d, *J* = 6.9 Hz, 6H), 2.26 (s, 3H), 3.90 (s, 3H), 4.07 (m, 1H), 11.65 (s, 1H). ^{13}C-NMR ($CDCl_3$, 100 MHz): δ 22.9, 24.7, 27.6, 51.9, 132.6, 151.9, 155.9, 162.3, 168.8. IE-MS (70 eV): 242 (M^+, 35), 140 ($C_6H_8N_2S^{\bullet}$, 100).

4.5.11. 2-acetamido-5-isopropylthiazole-4-carboxylic acid (**12**)

Compound **12** is obtained from **11** using the ester hydrolysis general procedure. White solid. Y= 100 %. M.p: 104 ºC decomp .^{1}H-NMR (DMSO-d_6, 400 MHz) δ 1.24 (d, *J* = 6.8 Hz, 6H), 2.09 (s, 3H), 3.99 (dt, *J* = 6.8 Hz, 1H), 12.25 (s, 1H), 12.74 (bp, 1H). ^{13}C NMR (DMSO-d_6, 100 MHz): δ 22.8, 25.2, 27.3, 135.1, 150.1, 153.8, 164.1, 169.1. IE-MS (70 eV): 228 (M^+, 20), 168 ($C_7H_8N_2OS^{\bullet}$, 56), 140 ($C_6H_8N_2S^{\bullet}$, 100).

4.5.12. Ethyl 2-(1-methyl-4-nitro-1H-pyrrole-2-carboxamido)thiazole-4-carboxylate (**13**)

Compound **13** was obtained from **4** and **5** using the general procedure for amide bond formation. The crude is purified using EtOAc:Hexanes (3:2) as eluent. White solid. R_f = 0.41. R = 62 %. M.p.: 215-217 °C. ^{1}H-NMR (DMSO-d_6, 400 MHz): δ 1.30 (t, *J* = 6.9 Hz, 3H), 3.99 (s, 3H), 4.29 (q, *J* = 6.9 Hz, 2H), 8.02 (d, *J* = 1.9 Hz, 1H), 8.11 (s, 1H), 8.30 (d, *J* = 1.9 Hz, 1H), 12.97 (s, 1H). ^{13}C-NMR ($CDCl_3$, 100 MHz): δ 14.7, 38.5, 61.1, 111.1, 123.6, 124.1, 130.4, 134.6, 141.5, 158.5, 158.8, 161.5.

4.5.13. Methyl 5-isopropyl-2-(1-methyl-4-nitro-1H-pyrrole-2-carboxamido)thiazole-4-carboxylate (**14**)

Compound **14** was obtained from **4** and **6** using the general procedure for amide bond formation, the crude was purified using EtOAc:$CHCl_3$ (1:4) as eluent. White solid. R_f = 0.51.

R = 87 %. M.p.: 118-120 °C. ^{1}H-NMR ($CDCl_3$, 400 MHz): δ 1.38 (d, *J* = 6.6 Hz, 6H), 3.72 (s, 3H), 4.10 (m, 4H), 7.11 (d, *J* = 1.9 Hz, 1H), 7.65 (d, *J* = 1.9 Hz, 1H), 11.13 (s, 1H). ^{13}C-NMR ($CDCl_3$, 100 MHz): δ 24.8, 27.8, 38.2, 51.8, 109.6, 124.0, 127.9, 133.7, 135.2, 153.6, 154.6, 158.3, 162.2.

4.5.14. Methyl 2-(4-(2-acetamido-5-isopropylthiazole-4-carboxamido)-1-methyl-1H-pyrrole-2-carboxamido)-5-isopropylthiazole-4-carboxylate (**15**) [11]

Compound **13** was reduced using the general procedure for nitro group reduction, and then coupled with **12** using the general procedure for amide bond formation. The reaction is purified using EtOAc as eluent. White solid. R_f = 0.4. Y = 30 %. M.p.: 170-171 °C. ^{1}H-NMR ($CDCl_3$, 400 MHz): δ 0.99 (d, *J* = 7.1 Hz, 6H), 1.38 (d, *J* = 7.1 Hz, 6H), 1.85 (s, 3H), 3.91 (s, 3H), 4.04 (s, 3H), 4.14 (dt, *J*= 7.1 Hz, 1H), 4.96 (m, 1H), 6.56 (d, *J* = 1.48 Hz, 1H), 6.71 (d, *J* = 1.48 Hz, 1H), 9.52 (s, 1H). ^{13}C-NMR ($CDCl_3$, 100 MHz): δ 20.8, 23.2, 24.8, 27.7, 37.4, 44.8, 52.1, 114.3, 122.0, 122.4, 128.7, 133.5, 153.1, 153.8, 158.1, 162.7, 171.1.

4.5.15. Methyl 2-(4-(2-((tert-butoxycarbonyl)amino)-5-isopropylthiazole-4-carboxamido)-1-methyl-1H-pyrrole-2-carboxamido)-5-isopropylthiazole-4-carboxylate (**16**)

Compound **14** was reduced using the general procedure for nitro group reduction, and then coupled with **9** using the general procedure for amide bond formation. The reaction is purified using EtOAc:Hexanes (6:4) as eluent. White solid. M.p.: 263 ºC decomp. Y = 40 %. ^{1}H-NMR ($CDCl_3$, 400 MHz): δ 1.34 (m, 12H), 1.56 (s, 9H), 3.90 (s, 3H), 3.97 (s, 3H), 4.12 (dt, *J* = 6.8 Hz, 1H), 4.37 (dt, *J* = 6.8 Hz, 1H), 6.63 (s, 1H), 7.62 (s, 1H), 8.40 (s, 1H), 9.02 (s, 1H), 9.56 (s, 1H). ^{13}C-NMR (DMSO-d_6, 100 MHz): δ 24.8, 24.9, 27.1, 27.6, 28.2, 37.1, 52.0, 83.1, 104.7, 120.3, 122.1, 122.2, 133.4, 135.3, 148.9, 152.2, 152.8, 154.1, 154.6, 158.3, 159.8, 162.8. EI-MS (20 eV): 590 (M^+, 0.1), 490 ($C_{21}H_{26}N_6O_4S_2$, 100), 322 ($C_{14}H_{18}N_4O_3S$, 43), 291 ($C_{13}H_{15}N_4O_2S^{\bullet}$, 80). IR KBr ν ($cm^{-1}$): 3351, 3124, 2915, 1765, 1491, 1101.

4.5.16. Ethyl 2-(4-(2-((tert-butoxycarbonyl)amino)thiazole-4-carboxamido)-1-methyl-1H-pyrrole-2-carboxamido)thiazole-4-carboxylate (**17**) [51]

Compound **17** was reduced using the general procedure for nitro group reduction, and then coupled with **6** using the general procedure for amide bond formation. The reaction is purified using $CHCl_3$:EtOAc (1:2). R_f = 0.51. White solid. R = 35 %. M.p.: 142 ºC. ^{1}H-NMR ($CDCl_3$, 400 MHz): δ 1.34 (t, *J* = 7.1 Hz, 3H), 1.55 (s, 9H), 3.95 (s, 3H), 4.35 (q, *J* = 7.1 Hz, 1H), 6.88 (s, 2H), 7.60 (d, 1H, *J* = 1.97 Hz), 7.79 (s, 1H), 7.80 (s, 1H), 8.72 (s, 1H), 8.90 (s,

1H), 9.78 (s, 1H). ^{13}C-NMR ($CDCl_3$, 100 MHz): δ 14.2, 28.1, 37.2, 61.4, 104.6, 117.9, 120.0, 120.3, 121.9, 122.3, 141.5, 158.1, 158.3, 158.4, 159.4, 161.1, 161.5.

4.5.17. 2-(4-(2-acetamido-5-isopropylthiazole-4-carboxamido)-1-methyl-1H-pyrrole-2-carboxamido)-5-isopropylthiazole-4-carboxylic acid (**18**)

Compound **18** was obtained from **15** using the general procedure for ester hydrolysis. White solid. Y = 100 %. M.p.: 122 ºC decomp. ^{1}H-NMR ($CDCl_3$, 400 MHz): δ 1.04 (d, *J* = 7.1 Hz, 6H), 1.40 (d, *J* = 7.1 Hz, 6H), 1.92 (s, 3H), 4.10 (s, 3H), 4.25 (dt, *J* = 7.1 Hz, 1H), 4.98 (dt, *J* = 7.1 Hz, 1H), 6.74 (d, *J* = 1.4 Hz, 1H), 7.39 (d, *J* = 1.4 Hz, 1H), 12.52 (s, 1H), 15.32 (s, 1H). ^{13}C-NMR ($CDCl_3$, 100 MHz): δ 20.9, 23.4, 24.4, 27.7, 37.9, 44.8, 116.2, 122.0, 122.4, 128.8, 132.6, 153.1, 156.6, 159.1 166.3, 170.9. ^{1}H-NMR (DMSO-d_6, 400 MHz): δ 1.29 (m, 12H), 2.13 (s, 3H), 3.90 (s, 3H), 4.05 (m, 1H), 4.16 (m, 1H), 7.35 (d, *J* = 1.4 Hz, 1H), 7.56 (d, *J* = 1.4 Hz, 1H), 9.61 (s, 1H), 12.15 (s, 1H), 12.45 (bp, 2H). EI-MS (70 eV); 518 (M^+,5), 474 ($C_{20}H_{22}N_6O_4S_2^{\bullet}$,15), 333 ($C_{15}H_{17}N_4O_3S^{\bullet}$, 42), 211 ($C_9H_{11}N_2O_2S^{\bullet}$, 100).

4.5.18. 2-(4-(2-((tert-butoxycarbonyl)amino)-5-isopropylthiazole-4-carboxamido)-1-methyl-1H-pyrrole-2-carboxamido)-5-isopropylthiazole-4-carboxylic acid (**19**)

Compound **19** was obtained from **16** using the general procedure for ester hydrolysis. White solid. Y = 100 %. M.p.: 254-256 ºC. ^{1}H-NMR (DMSO-d_6, 400 MHz): δ 1.27 (m, 12H), 1.48 (s, 9H), 3.88 (s, 3H), 4.02 (dt, *J* = 7.1 Hz, 1H), 4.15 (dt, *J* = 7.1 Hz, 1H), 7.32 (s, 1H), 7.55 (s, 1H), 9.49 (s, 1H), 11.49 (s, 1H), 12.31 (s, 1H), 12.71 (s, 1H). ^{13}C-NMR (DMSO-d_6, 100 MHz): δ 25.1, 25.2, 26.8, 27.2, 28.3, 37.1, 81.9, 107.5, 120.7, 121.8, 122.6, 136.6, 146.1, 150.0, 154.3, 154.9, 155.7, 159.6, 164.1. EI-MS (20 eV): 476 ($C_{20}H_{24}N_6O_4S_2$, 14), 432 ($C_{19}H_{24}N_6O_2S_2$, 62) 291 ($C_{13}H_{15}N_4O_2S^{\bullet}$, 100), 264 ($C_{12}H_{16}N_4O_S$, 45). IR KBr ν ($cm^{-1}$): 2935,2831, 1677, 1607, 1451,946.

4.5.19. 2-(4-(2-((tert-butoxycarbonyl)amino)thiazole-4-carboxamido)-1-methyl-1H-pyrrole-2-carboxamido)thiazole-4-carboxylic acid (**20**)

Compound **20** was obtained from **17** using the general procedure for ester hydrolysis. Pale yellow solid. Y = 100 %. M.p.: 198 ºC. ^{1}H-NMR (DMSO-d_6, 400 MHz): δ 1.49 (s, 9H), 3.90 (s, 1H), 7.38 (d, *J* = 1.6 Hz, 1H), 7.54 (d, *J* = 1.6 Hz, 1H), 7.84(s, 1H), 7.96 (s, 1H), 9.71 (s, 1H), 11.67 (s, 1H), 12.55 (s, 1H), 12.83 (bp, 1H). ^{13}C-NMR (DMSO-d_6, 100 MHz): δ 28.3, 37.2, 79.6, 107.9, 117.7, 120.7, 122.3, 142.6, 145.1, 158.6, 158.8, 159.6, 160.1, 162.7. EI-MS

(20 eV): 492 (M^+, 0.01), 349 ($C_{15}H_{17}N_4O_4S^{\bullet}$, 10), 249 ($C_{10}H_9N_4O_2S^{\bullet}$,100), 241 ($C_9H_{11}N_3O_3S\bullet$, 5). IR KBr ν ($cm^{-1}$) = 3148, 2971, 2932, 1663, 1491,1311.

4.6. Biological methods

4.6.1. Viability assays for T. b. brucei and murine macrophages

The bloodstream form of *T. b. brucei* (monomorphic strain 427) expressing an ectopic copy of the redox biosensor hGrx1-roGFP2 [29] (cell line 449_Grx-roGFP2) [19] was grown in HMI-9 medium complemented with 10 % v/v Fetal Bovine Serum (FBS, GIBCO®), 10 U/mL penicillin, 10 μg/mL streptomycin, 0.2 μg/mL bleomycin and 5 μg/mL hygromycin. Expression of the biosensor was induced by adding oxytetracycline (end concentration 1 μg/mL) to the culture medium. Cells were incubated aerobically in a humidified incubator containing 5% CO_2 at 37 ºC. Working solutions of the compounds were prepared at different concentrations in 100% (v/v) DMSO and the concentration of vehicle in the assay never exceeded 1% (v/v). The screening was performed at a fixed compound concentration of 5 μM whereas for EC_{50} determinations the concentrations tested ranged from 0.0001 to 120 μM. Controls included cells treated with DMSO 1% (v/v), 10 μM nifurtimox or 78 nM suramin. Parasite viability was evaluated as described by Maiwald *et al*. [52]. Briefly, 200 μL of a cell suspension containing 5×10^5 parasites/mL in exponential growth phase was seeded per well in a 96-well culture plate, then 2 μL from each compound was added per well and the culture plates were incubated at 37 ºC, 5% CO_2 for 24 h. Next, 50 μL from each well was transferred to a 96 U bottom well plate containing 100 μL of PBS 1X glucose [1% (w/v)], 2 μg/mL propidum iodide (PI) and analyzed in an Accuri™C6 (BD) flow cytometer (laser/filter pairs: $\lambda_{ex/em}$ = 488 nm / 540±85 nm). The data were analyzed with the Accuri C6 software (BD).

Murine macrophages (cell line J774, ATCC® TIB-67™) were cultivated in DMEM medium supplemented with FBS [10% (v/v)], 10 U/ mL penicillin and 10 μg/mL streptomycin, at 37 ºC, 5% CO_2 in a humidified incubator. Cell viability was determined from triplicates of 6-point concentrations of compounds, using the WST-1 reagent and the protocol described by Demoro *et a*l. [53].

For all assays, at least three experimental replicates were analyzed and cell viability was calculated as follows: viability(%) = 100 x (number of cells for compound Y at concentration X/ number of cells in the DMSO-treated control).

EC_{50} values were obtained from dose/response curves using a nonlinear fitting. The error is expressed as S.D. (corresponding to σ^{n-1}).

4.6.2. Membrane permeability assay

Two million parasites/mL were incubated with **16** (12 nM) and **17** (7 nM), DMSO [1% (v/v), negative control] and Triton X-100 [0.001% (v/v), positive control]. Culture samples were taken at different time points, diluted with PBS 1X glucose [1% (w/v)], added of PI (final concentration of 2 μg/mL) and analyzed by flow cytometry as described above. Results are expressed as mean ± S.D. (n = 3).

4.6.3. Intracellular redox state assay

Two million parasites/mL were incubated with **16** (59 and 12 nM), **17** (36 and 7 nM) or DMSO [1% (v/v)] for 4 h. For calibrating the biosensor, non-treated parasites were incubated for 20 min with DTT (1 mM), menadione (250 μM) or diamide (250 μM). In order to exclude dead cells from the analysis, PI was added at 2 μg/mL immediately prior to sample analysis by flow cytometry (Accuri™C6, BD). The following laser/filter pairs: $\lambda_{ex/em}$ = 488 nm / 530±33 nm for hGrx-roGFP2 and $\lambda_{ex/em}$ = 488 nm / 613 ± 30 nm for PI were used. The data were processed and analyzed with the Accuri C6 software. Results are expressed as mean ± S.D. (n = 3).

4.6.4. Cell cycle analysis

Parasites in exponential growth phase were plated at a density of 5×10^5 cells/mL and incubated for 6 h with hidroxyurea at 10 μg/mL. Next, cells were centrifuged (2000 *g*, 10 min at room temperature), washed twice with PBS 1X (10 mL) and then seeded back on a 6-well plate at a density of 5×10^5 parasites/mL. **16** (7 nM), **17** (14 nM), DAC (41 nM) or DMSO [1% (v/v)] were immediately added and cultures incubated for 18 h and 24 h at 37°C / 5% CO_2. Cells were centrifuged and washed thrice with PBS 1X (1 mL). Then the pellet was resuspended gently in EtOH [70% (v/v) in PBS 1X] and incubated overnight at 4º C. Finally, parasites were centrifuged, washed twice with PBS 1X (1 mL), resuspended in PBS 1X containing RNAse A (30 μg/mL, Fermentas) and incubated for 30 min at 37 ºC. PI was added at 2 μg/mL to stain nucleic acids. The samples were analyzed by flow cytometry as described above. Cell cycle analysis was performed using the ModFit LT software. Results are expressed as mean ± S.D. (estimated as σ^{n-1}, n=2).

4.6.5. Epifluorescence microscopy

Parasites cultured as described before and treated with DMSO [1% (v/v)], DAC (41 nM), **16** (12 nM) or **17** (7 nM) for 24 h were centrifuged (2000 *g*, 10 min) and washed twice with PBS 1X (1 mL). The pellet was resuspended in paraformaldehyde [4% (v/v) in PBS 1X] to a cell density of 4×10^4 parasites/μL and further incubated for 18 min at room temperature. After washing thrice with PBS 1X (1 mL), parasites were resuspended in PBS 1X at a density of 4×10^4 cells/μL and smeared on a glass slide. The slides were incubated protected from light for about 18 h at 4 ºC and then mounted using a Fluoroshield™ (Sigma-Aldrich) solution containing DAPI. Samples were analyzed by epifluorescence microscopy using 60X and 100X objectives with an OLYMPUS IX81 microscope. At least 50 cells were analyzed for each sample.

4.6.6. DNA-binding competition assays

Synthesis of kDNA and insertion into pUC18 plasmid (construct pUC18 kDNA) was ordered to GENSCRIPT. pUC18 and pUC18 kDNA (ampicillin resistance) were produced and isolated from *Escherichia coli* XL-1 using the PureLink™ Maxiprep Extraction Kit (Invitrogen). Purity and concentration were analyzed in a NanoDrop 1000 Spectrophotometer (Thermo Scientific) at 260 nm and by agarose gel electrophoresis [1% (w/v)] in TAE 0.5 X buffer at 135 mV, using λHindIII (Thermo Scientific) and a 1-Kb DNA-ladder (Invitrogen). Plasmids were dissolved in PBS 1X buffer (pH = 7.4) at 5 nM and incubated for 0.5 and 2 h with 20 μM DAC, **16**, **17**, or vehicle alone [DMSO 1% (v/v)]. Then DAPI (500 nM final concentration) was added and the emission spectra was recorded in a Cary Spectrofluorimeter ($\lambda_{ex/em}$ = 358 nm / 368-600 nm, using a 5 nm slit filter and the PMT at 700 mV). The fluorescence of the test samples was normalized against the control sample containing DNA, DMSO and DAPI, set at 100 %. Results are expressed as mean ± S.D. (σ^{n-1}) for n = 3.

4.6.7. Therapeutic efficacy study

Animal assays were carried employing procedures approved by the Animal Use and Ethic Committee (CEUA) of the Institut Pasteur de Montevideo (Protocol 004-12), which are in accordance with the Federation of European Laboratory Animal Science Association (FELASA) guidelines and the National law for Laboratory Animal Experimentation (Law nr. 18.611). Six to eight weeks-old female BalB/cJ mice (n = 24) weighing about 20 g were infected intraperitoneally with 10^4 parasites (bloodstream form of *T. b. brucei* strain AnTaT 1.1). At day 4^{th} post-infection, mice were randomly divided in 4 groups (n = 6/group) and administered intraperitoneally with 300 μL (prepared in 1 X PBS) of **17** at 1000X (8.36

mg/Kg × day × 7 days) or 250X (2.09 mg/Kg × day × 7 days), DMSO 3.3 mg/Kg × day ×7 days or a single dose of DAC at 40 mg/Kg. Parasitemia (determined by cell counting in a light microscope of blood samples extracted from the submandibular vein) and animal health status were controlled regularly as described earlier [54]. Animals displaying an impaired health status or parasitemia higher than 10^9 parasites/mL were sacrificed for ethical reasons.

4.6.8. Inactivation of **17** *by serum samples*

A solution of **17** at 100 μM prepared in fresh or heat-inactivated (54 ºC for 45 min) serum containing a maximal DMSO concentration of 1% (v/v) was incubated at 37 ºC for 24 h. The biological activity of both samples of **17** against *T. brucei* (cell line 449-hGrx-roGFP2) was tested at a final compound concentration of 10 and 1000 nM, and according to the method described in section *4.6.1*.

4.6.9. Statistical Analysis

All data here reported were plotted and analysed using the GraphPad Prism software (version 6.01). The statistical tests applied and the *p* values obtained are indicated in the respective figures.

Acknowledgements

J.F. acknowledges the support of ANII – Uruguay (POS_NAC_2014_1_102739). The technical support of staff from the Cell Biology Unit, Institut Pasteur de Montevideo, is gratefully acknowledged. The support of CSIC Grupos (UdelaR) and PEDECIBA (Uruguay) is gratefully acknowledged by L.S.. All funding sources were not involved in study design, collection, analysis and interpretation of data; in the writing of the paper; and in the decision to submit the article for publication.

References

[1] R. Brun, J. Blum, F. Chappuis, C. Burri, Human African Trypanosomiasis, Lancet 375 (2010) 148–159.

[2] World Health Organization, Third WHO Report on Neglected Tropical Diseases. Investing to Overcome the Global Impact of Neglected Tropical Diseases, 2015, ISBN 978 92 4 156486 1 (Accessed November 6th 2019), http://www.who.int/neglected_diseases/9789241564861/en/.

[3] F. Giordani, L.J. Morrison, T.G. Rowan, H.P. de Koning, M.P. Barrett, The animal

trypanosomiases and their chemotherapy: a review, Parasitology 143 (2016) 1862–1889.

[4] A.P. Shaw, G. Cecchi, G.R. Wint, R.C. Mattioli, T.P. Robinson, Mapping the economic benefits to livestock keepers from intervening against bovine trypanosomosis in Eastern Africa, Preventive Veterinary Medicine 113 (2014) 197–210.

[5] I.A Teka, A.J. Kazibwe, N. El-Sabbagh, M.I. Al-Salabi, C.P. Ward, A.A. Eze, J.C. Munday, P. Maser, E. Matovu, M.P. Barrett, H.P. de Koning, The diamidine diminazene aceturate is a substrate for the high-a□nity pentamidine transporter: implications for the development of high resistance levels in trypanosomes, Molecular Pharmacology 80 (2011) 110–116.

[6] V.K.B.K. Mesu, W.M. Kalonji, C. Bardonneau, O.V. Mordt, S. Blesson, F. Simon, S. Delhomme, S. Bernhard, W. Kuziena, J.P.F. Lubaki, et al., Oral fexinidazole for late-stage African Trypanosoma brucei gambiense trypanosomiasis: a pivotal multicentre, randomised, non-inferiority trial, Lancet 391 (2018) 1–11.

[7] R.J. Wall, E. Rico, I. Lukac, F. Zuccotto, S. Elg, I.H. Gilbert, Y. Freund, M.R.K. Alley, M.C. Field, S. Wyllie, D. Horn, Clinical and Veterinary Trypanocidal Benzoxaboroles Target CPSF3, Proc. Natl. Acad. Sci. 115 (2018) 9616–9621.

[8] M.L. Kopka, C. Yoon, D. Goodsell, P. Pjura, R.E. Dickerson, The molecular origin of DNA-drug specificity in netropsin and distamycin, Proc. Natl. Acad. Sci. U. S. A. 82 (1985) 1376–1380.

[9] C.H. Ríos Martínez, J.J. Nué Martínez, G.U. Ebiloma, H.P. de Koning, I. Alkorta, C. Dardonville, Lowering the pKa of a bisimidazoline lead with halogen atoms results in improved activity and selectivity against Trypanosoma brucei in vitro, Eur. J. Med. Chem. 101 (2015) 806–817.

[10] C.H. Ríos Martínez, L. Lagartera, C. Trujillo, C. Dardonville, Bisimidazoline arylamides binding to the DNA minor groove: N1-hydroxylation enhances binding affinity and selectivity to AATT sites. Med. Chem. Commun. 6 (2015) 2036–2042.

[11] D.L. Boger, B.E. Fink, M.P. Hedrick, Total synthesis of distamycin A and 2640 analogues: a solution-phase combinatorial approach to the discovery of new, bioactive DNA binding agents and development of a rapid, high-throughput screen for determining relative DNA binding affinity or DNA binding sequence selectivity, J. Am. Chem. Soc. 122 (2000) 6382–6394.

[12] F.J. Scott, A.I. Khalaf, F. Giordani, P.E. Wong, S. Duffy, M. Barrett, V.M. Avery, C.J. Suckling, An evaluation of minor groove binders as anti-Trypanosoma brucei brucei therapeutics, Eur. J. Med. Chem. 116 (2016) 116–125.

[13] A.I. Khalaf, A.R. Pitt, M. Scobie, C.J. Suckling, J. Urwin, R.D. Waigh, R.V. Fishleigh, C. Young, W.A. Wylie, The synthesis of some head to head linked DNA minor groove binders, Tetrahedron Lett. 56 (2000) 5225–5239.

[14] A.I. Khalaf, R.D. Waigh, A.J. Drummond, B. Pringle, I. Mcgroarty, G.G. Skellern, C.J. Suckling, Distamycin analogues with enhanced lipophilicity : synthesis and antimicrobial activity, J. Med. Chem. 47 (2004) 2133–2156.

[15] S. Lang, A.I. Khalaf, D. Breen, J.K. Huggam, C.J. Clements, S.P. MacKay, C.J. Suckling, Oligoamides of 2-amino-5-alkylthiazole 4-carboxylic acids : anti-trypanosomal compounds, Med. Chem. Res. 23 (2014) 1170–1179.

[16] D. Drozdowkska, The analogues of DNA minor-groove binders as antineoplastic compounds, In: Breast Cancer - Current and Alternative Therapeutic, E. Gunduz Ed., InTech (2011) 133–149.

[17] N.G. Anthony, D. Breen, J. Clarke, G. Donoghue, A.J. Drummond, E.M. Ellis, C.G. Gemmell, J.J. Helesbeux, I.S. Hunter, A.I. Khalaf, et al., Antimicrobial lexitropsins containing amide, amidine, and alkene linking groups, J. Med. Chem. 50 (2007) 6116–6125.

[18] M.P. Barrett, C.G. Gemmell, C.J. Suckling, Minor groove binders as anti-infective agents, Pharmacol. Ther. 139 (2013) 12–23.

[19] J. Franco, A. Medeiros, D. Benítez, K. Perelmuter, G. Serra, M. A. Comini, L. Scarone, In vitro activity and mode of action of distamycin analogues against African Trypanosomes, Eur. J. Med. Chem. 126 (2017) 776–788.

[20] W.D. Cooper, Synthesis of 2-trifluoroacetylpyrrole, J. Org. Chem. 23 (1958) 1382.

[21] A. Delgado, J. Clardy, Aryl trifluoromethyl ketones as hydrates as precursors of carboxylic acids and esters, Tetrahedron Lett. 33 (1992) 2789–2790.

[22] A. Hantzsch, J.E. Weber, Ueber verbindungen des thiasola (pyridine der thiophenreihe), Dtsch. Chem. Gesellschaft 20 (1887) 3118–3132.

[23] A. Barton, S.P. Breukelman, P.T. Kaye, G.D. Meakins, D.J. Morgan, The preparation of thiazole-4- and -5-carboxylates, and an infrared study of their rotational isomers, J. Chem. Soc. Perkin Trans. 1 (1982) 159–164.

[24] R.P. Karuvalam, K.R. Haridas, S.K. Nayak, T.N. Guru, P. Rajeesh, R. Rishikesan, N.S. Kumari, Design, synthesis of some new (2-Aminothiazol-4-Yl) methylester derivatives as possible antimicrobial and antitubercular agents, Eur. J. Med. Chem. 49 (2012) 172–182.

[25] L. Forlani, A.L. Tocke, E. del Vecchio, S. Lakhdar, R. Goumont, F. Terrier, Assessing the nitrogen and carbon nucleophilicities of 2-aminothiazoles through coupling with superelectrophilic 4,6-dinitrobenzofuroxan, J. Org. Chem. 71 (2006) 5527–5537.

[26] F. Forlani, M. Sintoni, Catalytic effects in aromatic nucleophilic substitution reactions. Reactions between 1-fluoro-2,4-dinitrobenzene and 2-aminothiazole derivatives, J. Chem. Soc. Perkin Trans. 2 11 (1988) 1959–1962.

[27] E.E. Baird, P.B. Dervan, Solid phase synthesis of polyamides containing imadizole and pyrrole amino acids, J. Am. Chem. Soc. 118 (1996), 6141–6146.

[28] J. Franco, F. Sardi, L. Szilágyi, K.E. Kövér, K. Fehér, M.A. Comini, Diglycosyl diselenides alter redox homeostasis and glucose consumption of infective African trypanosomes, *Int. J. Parasitol. Drugs Drug Resist. 7* (2017) 303–313.

[29] M. Gutscher, A.L. Pauleau, L. Marty, T. Brach, G.H. Wabnitz, Y. Samstag, A. J. Meyer, T.P. Dick, Real-time imaging of the intracellular glutathione redox potential,

Nat. Meth. 5 (2008) 553–559.

[30] B. Manta, M.N. Möller, M. Bonilla, M. Deambrosi, K. Grunberg, M. Bellanda, M.A. Comini, G. Ferrer-Sueta, Kinetic studies reveal a key role of a redox-active glutaredoxin in the evolution of the thiol-redox metabolism of trypanosomatid parasites, J. Biol. Chem. 294 (2019) 3235–3248.

[31] P.G. McKean, Coordination of cell cycle and cytokinesis in Trypanosoma brucei, Curr. Opin. Microbiol. *6* (2003) 600–607.

[32] N.G. Jones, E.B. Thomas, E. Brown, N.J. Dickens, T.C. Hammarton, J.C. Mottram, Regulators of Trypanosoma brucei cell cycle progression and differentiation identified using a kinome-wide RNAi screen, PLoS Pathog. 10 (2014) e1003886.

[33] R. Woodward, K. Gull, Timing of nuclear and kinetoplast DNA replication and early morphological events in the cell cycle of Trypanosoma brucei, J. Cell Sci. 95 (1990) 49–57.

[34] B. Musunda, D. Benítez, N. Dirdjaja, M.A. Comini, R.L. Krauth-Siegel, Glutaredoxin-deficiency confers bloodstream Trypanosoma brucei with improved thermotolerance, Mol. Biochem. Parasitol. 204 (2015) 93–105.

[35] T.A. Shapiro, P.T. Englund, Selective cleavage of kinetoplast DNA minicircles promoted by antitrypanosomal drugs, *Proc. Natl. Acad. Sci. U. S. A. 87* (1990) 950–954.

[36] A.A. Zuma, D.P. Cavalcanti, M. Zogovich, A.C.L. Machado, I.C. Mendes, M. Thiry, A. Galina, W. de Souza, C.R. Machado, M.C.M. Motta, Unveiling the effects of berenil, a DNA-binding drug, on Trypanosoma cruzi: implications for KDNA ultrastructure and replication, Parasitol. Res. 114 (2014) 419–430.

[37] A. Schnaufer, G.J. Domingo, K. Stuart, Natural and induced dyskinetoplastic trypanosomatids: how to live without mitochondrial DNA, Int. J. Parasitol. 32 (2002) 1071–1084.

[38] L. de Oliveira Ramos Pereira, A. Brandão, An analysis of trypanosomatids kDNA minicircle by absolute dinucleotide frequency, Parasitol. Int. 62 (2013) 397–403.

[39] S. Neidle, DNA minor-groove recognition by small molecules, Nat. Prod. Rep. 18 (2001) 291–309.

[40] Y. Chai, M. Munde, A. Kumar, L. Mickelson, S. Lin, N.H. Campbell, M. Banerjee, S. Akay, Z. Liu, A.A. Farahat, et al., Structure-dependent binding of arylimidamides to the DNA minor groove, *Chem. Bio. Chem. 15* (2014) 68–79.

[41] N.A. Panat, B.G. Singh, D.K. Maurya, S.K. Sandur, S.S. Ghaskadbi, Troxerutin, a natural flavonoid binds to DNA minor groove and enhances cancer cell killing in response to radiation, Chem. Biol. Interact. 251 (2016) 34–44.

[42] S. Sbicego, E. Vassella, U. Kurath, B. Blum, I. Roditi, The use of transgenic Trypanosoma brucei to identify compounds inducing the differentiation of bloodstream forms to procyclic forms, Mol. Biochem. Parasitol. 104 (1999) 311–322.

[43] G. Liu, J. Xu, H. Wu, D. Sun, X. Zhang, X. Zhu, et al., IL-27 Signaling is crucial for

812 survival of mice infected with African trypanosomes via preventing lethal effects of
813 CD4+ T cells and IFN-γ, PLoS Pathog 11 (2015) e1005065.

814 [44] R. Mentlein, E. Heymann, Hydrolysis of ester- and amide-type drugs by the purified
815 isoenzymes of nonspecific carboxylesterase from rat liver, Biochem. Pharmacol. 33
816 (1984) 1243–1248.

817 [45] K. Murakami, Y. Takagi, K. Mihara, T. Omura, An isozyme is secreted of microsomal
818 from rat liver into the blood, J. Biochem. 66 (1993) 61–66.

819 [46] C.D. Sohaskey, A.G. Barbour, Esterases in serum-containing growth media counteract
820 chloramphenicol acetyltransferase activity in vitro, *Antimicrob. Agents Chemother. 43*
821 (1999) 655–660.

822 [47] A. Daina, O. Michielin, V. Zoete, SwissADME: A free web tool to evaluate
823 pharmacokinetics, drug-Likeness and medicinal chemistry friendliness of small
824 molecules, Sci. Rep. 7 (2017) 1–13.

825 [48] D.D. Perrin, W.L.F. Armarego, *Purification of laboratory chemicals*, Pergamon Press,
826 1988.

827 [49] M. Thomas, U. Varshney, S. Bhattacharya, Distamycin analogues without leading
828 amide at their N-termini-comparative binding properties to AT- and GC-rich DNA
829 sequences, Eur. J. Org. Chem. 2002 (2002) 3604–3615.

830 [50] E.K. Rao, Y. Bathini, J.W. Lown, Synthesis of novel thiazole-containing DNA minor
831 groove binding oligopeptides related to the antibiotic distamycin, J. Org. Chem. 55
832 (1990) 728–737.

833 [51] F. Brucoli, R.M. Hawkins, C.H. James, P.J.M. Jackson, G. Wells, T.C. Jenkins, T.
834 Ellis, M. Kotecha, D. Hochhauser, J.A. Hartley, et al., An extended
835 pyrrolobenzodiazepine − polyamide conjugate with selectivity for a DNA sequence
836 containing the ICB2 transcription factor binding site, J. Med. Chem. 56 (2013) 6339–
837 6351.

838 [52] F. Maiwald, D. Benítez, D. Charquero, M.A. Dar, H. Erdmann, L. Preu, O. Koch, C.
839 Hölscher, N. Loaëc, L. Meijer et al., 9- and 11-substituted 4-azapaullones are potent
840 and selective inhibitors of African trypanosoma, Eur. J. Med. Chem. 83 (2014) 274–
841 283.

842 [53] B. Demoro, C. Sarniguet, R. Sánchez-Delgado, M. Rossi, D. Liebowitz, F. Caruso, C.
843 Olea-Azar, V. Moreno, A. Medeiros, M.A. Comini, et al. New organoruthenium
844 complexes with bioactive thiosemicarbazones as co-ligands: potential anti-
845 trypanosomal agents, Dalt. Trans. 41 (2012) 1534–1543.

846 [54] M. Bonilla, E. Krull, F. Irigoín, G. Salinas, M.A. Comini, Selenoproteins of African
847 trypanosomes are dispensable for parasite survival in a mammalian host, Mol.
848 Biochem. Parasitol. 206 (2016) 13–19.

849

850

Figure legends

Scheme 1 Building block synthesis i) TFAA, Et_2O, 0 ºC, 6 h, 98 % ii) Ac_2O, HNO_3, 10 ºC, 3 h, 80 % iii) NaH, DMF:H_2O, 60 ºC, 3 h, 86 % iv) $(Boc)_2O$, TEA, 4-DMAP, CH_2Cl_2, reflux, 6 h, $Y_{\mathbf{7}}$: 100 %, 72 h $Y_{\mathbf{8}}$= 74 % v) KOH, H_2O:THF; $Y_{\mathbf{9,10}}$ = 100 % vi) Ac_2O, Py, reflux, 6 h, Y = 100 %.

Scheme 2 i) HBTU, DIPEA, 4-DMAP,**5** or **6** CH_2Cl_2, rt, 24 h $Y_{\mathbf{13}}$ = 87 % $Y_{\mathbf{14}}$ = 62 % ii) a) H_2/Pd (C), MeOH, rt, 3 h b) HBTU, DIPEA, 4-DMAP, **9**, **10** or **12**, CH_2Cl_2, rt, 24 h Y_{15} = 30 %, Y_{16} = 40 %, Y_{17} = 35 % iii) LiOH, MeOH:H_2O, rt, 24 h, $Y_{18,19,20}$ = 100 %.

Figure 1. Distamycin and analogues.

Figure 2. Plasma membrane integrity and intracellular redox state of African trypanosomes treated with *N*-methyl pyrrole bis-thiazoles. The bloodstream form of *T. b. brucei* (2×10^6 parasites/mL) was incubated 4 h with **16** and **17** at their EC_{50} (12 nM and 7 nM, respectively) or 5X EC_{50}. Thereafter, **A)** membrane integrity was assayed by the incorporation of propidium iodide and **B)** the intracellular redox state was assessed with a redox biosensor. Controls included parasites treated with vehicle (DMSO 1 %, v/v), Triton X-100 (0.001 %, v/v), a reducing (DTT 1 mM) and an oxidizing agent (Menadione 250 µM). For details in the protocol see section **4.6.3**. The results are expressed as mean ± S.D (n = 3). The asterisks denote the probability index (**** $p < 0.0001$; ONE WAY ANOVA analysis) compared to DMSO.

Figure 3. Cell cycle analysis of African trypanosomes treated with *N*-methyl pyrrole bis-thiazoles. The bloodstream form of *T. b. brucei* (5×10^5 parasites/mL) was incubated for 24 h with DMSO [1% (v/v)], **17** (7 or 14 nM) or with DAC (41 nM), and the cell populations with different DNA content analyzed by flow cytometry prior staining with PI. The results are represented as the average corresponding to three experimental replicates with an associated error in the determination ≤ 15%. The asterisks denote statistical difference (****, $p < 0.0001$) *vs*. DMSO according to a χ^2 contingency test.

Figure 4. DNA-content analysis by epifluorescence microscopy. *T. b. brucei* parasites (5×10^5 parasites/mL) were treated with DMSO (1 %, v/v), DAC (41 nM), **16** (12 nM) and **17** (7 nM) for 24 h, then stained with DAPI and analyzed by epifluorescence microscopy. **A)** Parasite populations classified according to their DNA-phenotype. Representative images (superposition of bright field and fluorescence) for DAPI-stained parasites treated with **B)**

DMSO, **C) 17** and **D)** DAC. At least 50 parasites were analyzed for each condition. N= nucleous, K= kinetoplast.

Figure 5. DAPI-competition assays for different DNA samples. Five nM DNA (pUC18 or pUC18kDNA dissolved in PBS 1X) were incubated with DMSO (1% v/v), 20 µM DAC, **16** or **17** (all prepared in PBS 1X with 1 % v/v DMSO) for **A)** 30 min and **B)** 120 min, and then DAPI was added at a final concentration of 0.5 µM. The emission spectra was recorded in a spectrofluorimeter ($\lambda_{ex/em}$ = 358 nm/368-600 nm). The fluorescence is expressed as percentage normalized against the maximum value (λ_{em} = 461 nm) obtained for the corresponding DNA + DMSO samples set at 100 %. Multiple comparison two-way ANOVA test were performed, where ** and ## denote statistical significance (p <0.01) when plasmids (pUC18 *vs.* pUC18kDNA) and incubation time (30 *vs.* 120 min), respectively, is compared for each treatment.

Figure 6. Parasitemia of *T. b. brucei*-infected mice treated with 17 and the control drug DAC. BalbC/J mice (n=6/group) were infected with 10^4 bloodstream *T. b. brucei* (strain Antat 1.1) and at day 4 post-infection were treated intraperitoneally with DMSO (3.3 mg/Kg × day/7 days), a single dose of DAC (40 mg/Kg) or (at 8.36 mg/Kg or 2.09 mg/Kg both doses applied daily during 7 days). The lower and higher dose of **17** are referred here as the 250X and 1000X, respectively, EC_{50} values determined in vitro. Parasitemia was assessed at different time-points by microscopy using a Neubauer chamber. The probability values are shown for groups with differences statistically significant with respect to the vehicle control group (DMSO), according to a non-parametric Kruskal-Wallis test.

Table 1. Anti-trypanosomal activity and selectivity of 13-20. The anti-proliferative activity of the compounds and control drugs (nifurtimox, suramin and diminazene aceturate: DAC) was assayed against bloodstream *T. b. brucei* and murine macrophages (cell line J774) after a 24 h exposure. The results are expressed as the mean ± SD (n = 3).

		Thiazole substituent			Infective *T. b. brucei*		
	Compound	**R_1**	**R_2**	**R_3**	**Viability (% ± SD) at 5 µM**	**EC_{50} ± SD (nM)**	**Selectivity index**
tri-thiazole	**1**[a]	Et	H	Boc	NR	310 ± 70	16
pyrrol-thiazole	**13**	Met	iPr	H	105.6 ± 8.2	ND	ND
	14	Et	H	H	120.5 ± 9.2	ND	ND
thiazole-pyrrol-thiazole	**15**	Met	iPr	Ac	5.4 ± 3,8	827 ± 350	> 35
	16	Met	iPr	Boc	15.5 ± 1.4	11.8 ± 3.8	>10169
	17	Et	H	Boc	0.06 ± 0.5	7.1 ± 1.3	5560
	18	H	iPr	Ac	113.1 ± 9.9	ND	ND
	19	H	iPr	Boc	48.5 ± 4.4	ND	ND
	20	H	H	Boc	23.6 ± 0.8	3325 ± 1425	> 145
	Nifurtimox					10000 ± 2000	10
	Suramin					78 ± 10	ND
	DAC					41 ± 5	ND

[a] Data reported in [19]

Table 2. Viability assay for *T. b. brucei* treated with **17** pre-incubated with fresh or heat-inactivated fetal bovine serum.

				inactivated serum			**fresh serum**		
17 (nM)	**0**	**10**	**1000**	**0**	**10**	**1000**	**0**	**10**	**1000**
Viability	100	54.1	10.7	98.5	104.6	17.5	100.0	84.2	17.2
± SD (%)	± 10	± 15.4	± 2.1	± 1.4	± 2.8	± 2.2	± 3.5	± 0.7	± 1.5

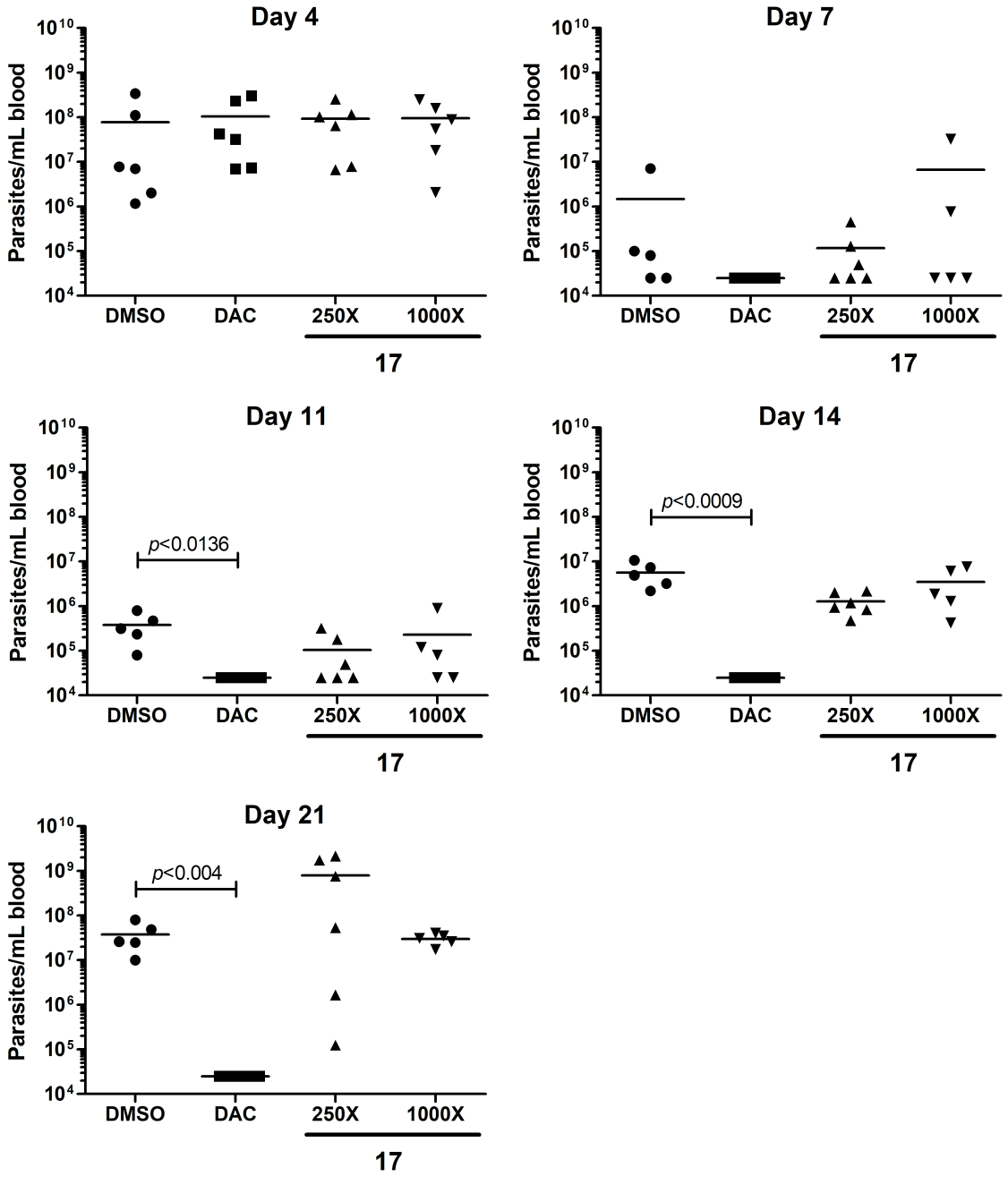
Day 4
Day 7
Day 11
Day 14
Day 21
Parasites/mL blood
10^{10}
10^{9}
10^{8}
10^{7}
10^{6}
10^{5}
10^{4}
DMSO
DAC
250X
1000X
17
p<0.0136
p<0.0009
p<0.004

Distamycin

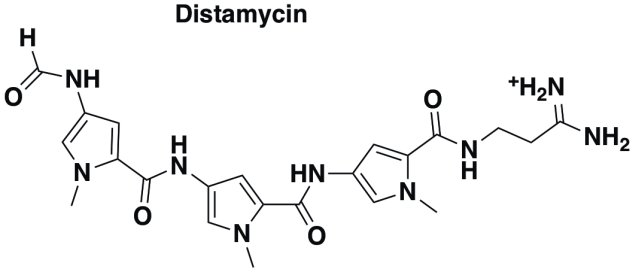

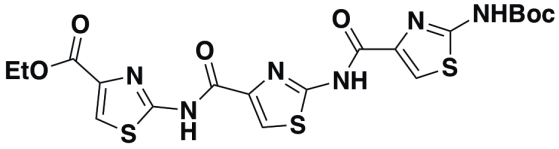

1

New series

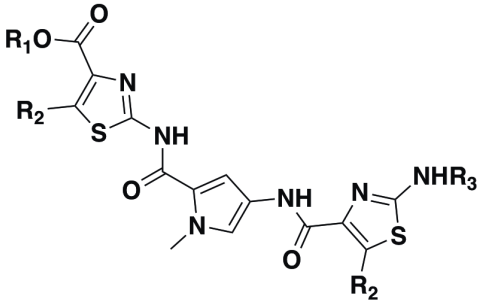

R_1 = H, Me, Et
R_2 = H, iPr
R_3 = Boc, Ac

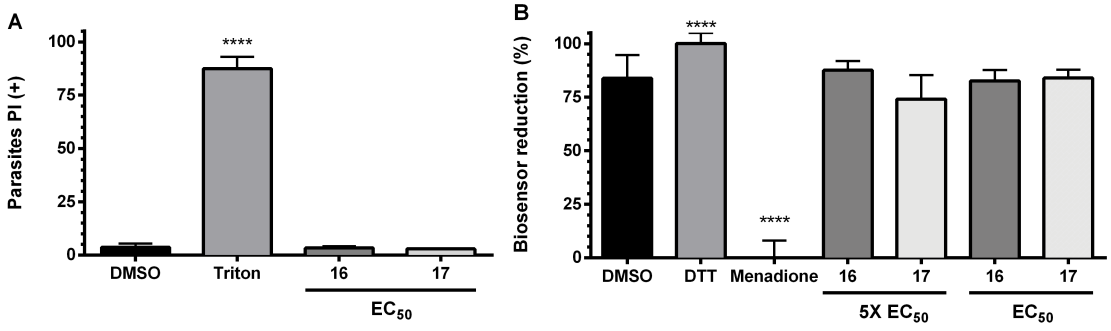
A
Parasites PI (+)
100
75
50
25
0
****
DMSO
Triton
16
17
EC50
B
Biosensor reduction (%)
100
75
50
25
0
****
****
DMSO
DTT
Menadione
16
17
16
17
5X EC50
EC50

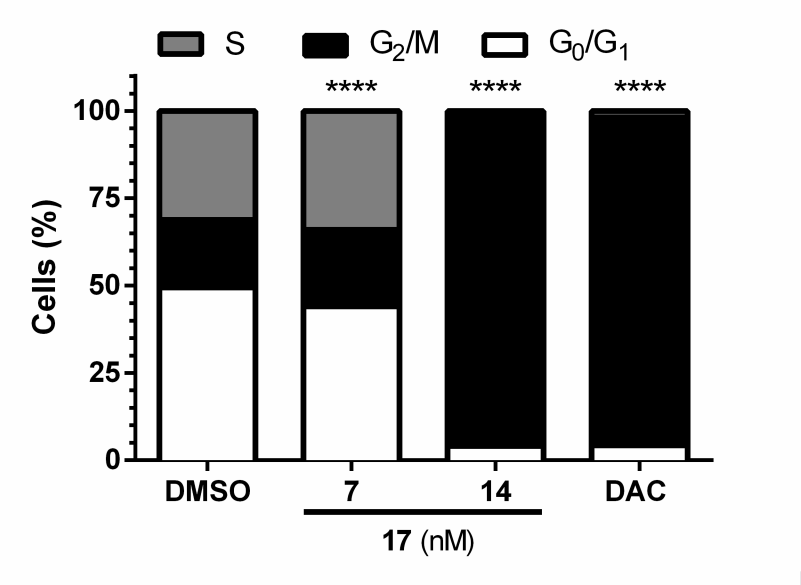

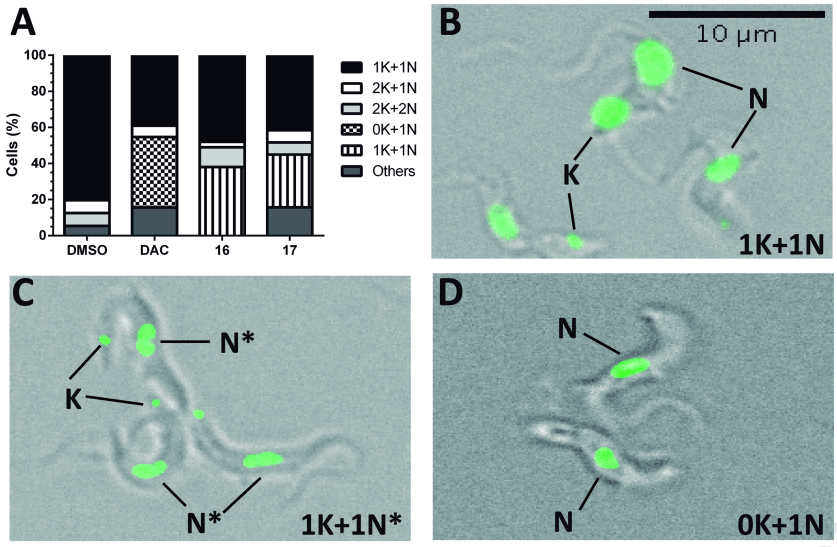

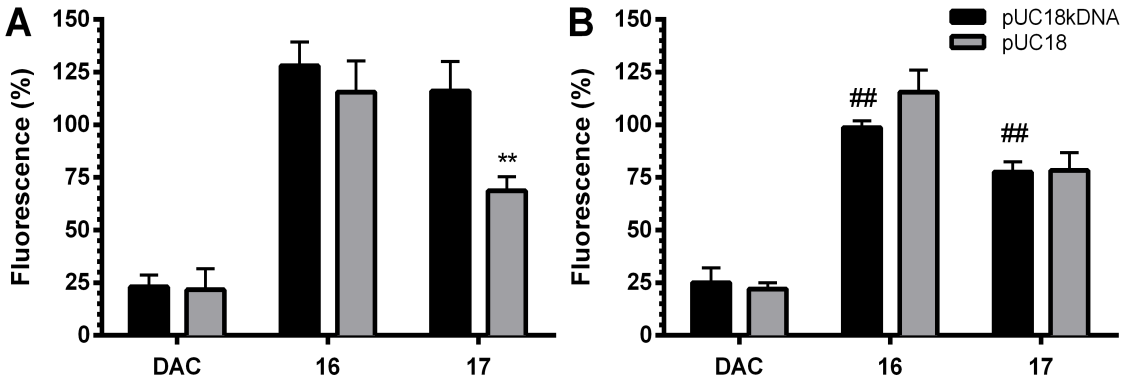
A
Fluorescence (%)
150
125
100
75
50
25
0
DAC
16
17
**
B
Fluorescence (%)
pUC18kDNA
pUC18
##
##
DAC
16
17

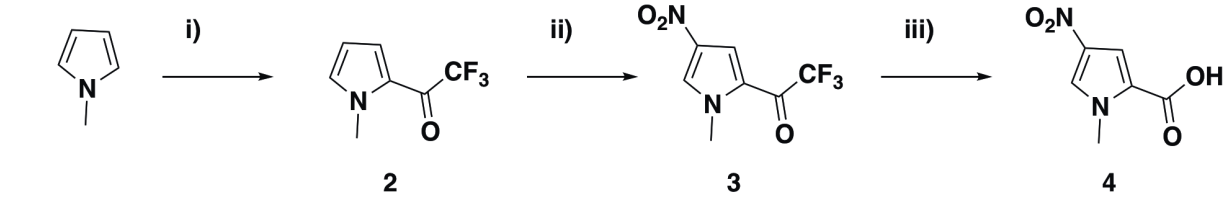

2 3 4

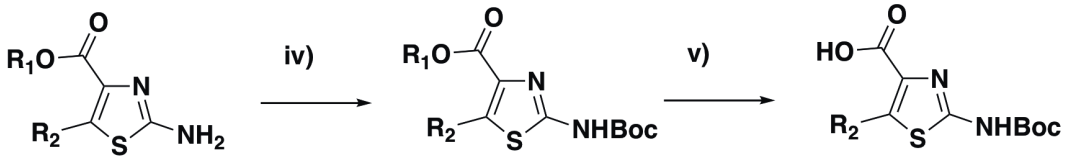

5 (R_1 = Me, R_2 = iPr)
6 (R_1 = Et, R_2 = H)

7 (R_1 = Me, R_2 = iPr)
8 (R_1 = Et, R_2 = H)

9 (R_2 = iPr)
10 (R_2 = H)

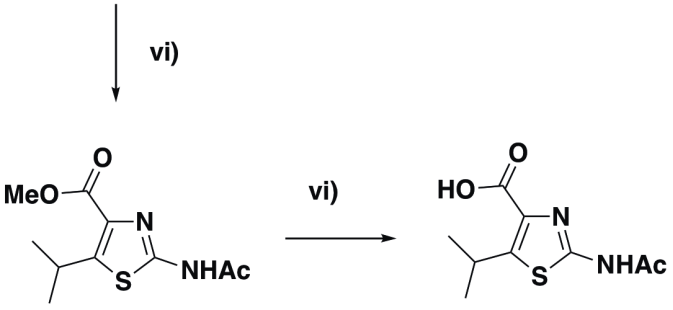

11 12

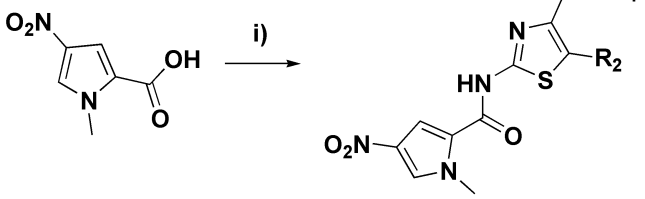

13 (R_1 = Me, R_2 = iPr)
14 (R_1 = Et, R_2 = H)

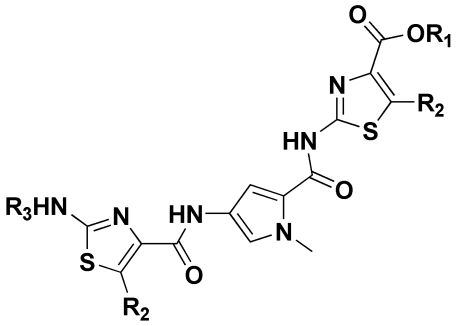

15 (R_1 = Me, R_2 = iPr, R_3 = Ac)
16 (R_1 = Me, R_2 = iPr, R_3 = Boc)
17 (R_1 = Et, R_2 = H, R_3 = Boc)

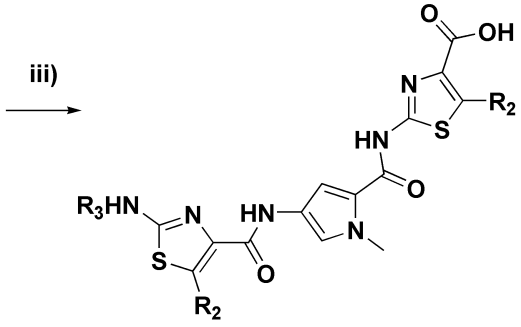

18 (R_2 = iPr, R_3 = Ac)
19 (R_2 = iPr, R_3 = Boc)
20 (R_2 = H, R_3 = Boc)

Highlights

• bis-thiazoles with a central pyrrole ring show low nM potency and high selectivity against *Trypanosoma brucei*

• terminal amine and carboxylic acid must be protected to increase biological activity

• trypanostatic action involves inhibition of parasite´ mitochondrial DNA replication

• the compounds do not induce DNA-degradation and show an atypical interaction with the target DNA

Declaration of interests

☒ The authors declare that they have no known competing financial interests or personal relationships that could have appeared to influence the work reported in this paper.

☐The authors declare the following financial interests/personal relationships which may be considered as potential competing interests: